Available online at www.sciencedirect.com
ScienceDirect
Trans. Nonferrous Met. Soc. China 24(2014) 2295−2300
Transactions of Nonferrous Metals Society of China
www.tnmsc.cn

Effects of T9I6 thermo-mechanical process on microstructure, mechanical properties and ballistic resistance of 2519A aluminum alloy

Gang GU[1,2], Ling-ying YE[1,2], Hai-chun JIANG[1,2], Da-xiang SUN[1,2], Pan ZHANG[1,2], Xin-ming ZHANG[1,2]

1. School of Materials Science and Engineering, Central South University, Changsha 410083, China;
2. Key Laboratory of Nonferrous Materials Science and Engineering, Ministry of Education, Central South University, Changsha 410083, China

Received 17 October 2013; accepted 23 April 2014

Abstract: The effects of T9I6 thermo-mechanical process on microstructures, mechanical properties and ballistic resistance of 2519A aluminum alloy were investigated by optical microscopy (OM), transmission electron microscopy (TEM), tensile tests and ballistic resistance test. After T9I6 treatment, the yield strength, tensile strength and elongation rate of 2519A aluminum alloy reach 501 MPa, 540 MPa and 14%, respectively. And the ballistic limit velocity of 2519A-T9I6 alloy (30 mm in thickness) is 715 m/s. The microstructure varies near the sidewalls of crater. The interrupted ageing contributes to these excellent properties of the alloy. During T9I6 process, the precipitation of Guinier Preston (GP) zone is finer and denser during the interrupted ageing, thus resulting in well precipitated strengthening phase.

Key words: 2519A aluminum alloy; T9I6 thermo-mechanical treatment; mechanical properties; microstructure; ballistic resistance

1 Introduction

2519 aluminum alloy (Al−5.56Cu−0.36Mg−0.44Mn−0.11Zr−0.07V−0.02Zn−0.14Fe−0.04Si; mass fraction, %) is a kind of plate armor material developed by Aloca in 1980s. It has been improved to a new version named 2519A (Al−5.80Cu−0.20Mg−0.30Mn−0.20Zr−0.20Fe−0.10Si, mass fraction, %) in China [1]. This 2519A alloy was used in T87 temper (7% cold rolling, then artificial ageing) with a proper combination of mechanical properties, ballistic resistance and resistance to stress corrosion cracking. 2519A alloy has been used extensively in naval structures, such as advanced amphibious assault vehicle (AAAV) [2].

However, with the development of weapons, aluminum alloy armor with a better service property is in desperate need. Studies on this issue have obtained certain achievements. ZHANG et al showed [3,4] that the tensile strength of 2519A aluminum alloy increased sharply from 470 MPa (T87 temper, cold-rolling at a reduction rate of 7%, then peak ageing) to 551 MPa (cold-rolling at a reduction rate of 80%, then peak ageing). The work hardening contributed to the increase of the tensile property mainly. However, with a severe plastic deformation, there was an unacceptable decrease in plasticity and toughness. Another way to improve the properties of the alloy is adding rare earth elements, which were working as micro-alloying elements, to influence the precipitation [5,6]. Studies showed that adding Ce [6] or Yb [7] at a proper amount could increase the tensile strength by about 25 MPa while the elongation rate was 10.7%. However, compared with the limited improvement, the cost of the rare earth could not be ignored. It could be found that both these 2 ways mentioned above could not improve the strength of the 2519A alloy while keeping the toughness and plasticity at a reasonable level. It is significant to find a new way to improve the comprehensive property of the 2519A aluminum alloy.

After LÖFFLER et al [8] reported a phenomenon called “secondary precipitation” in Al−Zn alloys in 1980s, it has been studied well and laid a foundation for interrupted ageing process [9−11]. Both of the T6I6 and T9I6 processes have been used to Al−Zn−Mg [12,13] alloys and Al−Li [14] alloys widely. The former works on interrupted ageing process were mainly about T6I4, T6I6 and T8I6 temper (‘I’ means interrupted

Foundation item: Project (2012CB619501) supported by the National Basic Research Program of China
Corresponding author: Ling-ying YE; Tel/Fax: +86-731-88830265; E-mail: lingyingye@csu.edu.cn
DOI: 10.1016/S1003-6326(14)63347-1

ageing). However, works about T9I6 have not been reported yet by now. Only the US patent mentioned the T9I6 process before. Both the effects and mechanisms need to be clarified.

The ballistic limit velocity (v_{50}) is the velocity required for a particular projectile (at least 50% of the time) to penetrate a particular piece of material reliably. In other words, a given projectile will not pierce a given target when the projectile velocity is lower than the ballistic limit.

This study introduced the interrupted ageing into the 2519A aluminum alloy to improve the comprehensive property. And the T9I6 process, which is one of the interrupted ageing methods, was studied. It aims at investigating the ballistic properties and dynamic response of the 2519A-T9I6 alloy. The microstructure and precipitates were observed to clarify the improvement in both quasi-static and dynamic states.

2 Experimental

Investigated 2519A alloys were provided by Southwest Aluminum Co., Ltd., China. The nominal composition of the alloy is listed in Table 1.

Table 1 Chemical composition of 2519A alloy (mass fraction, %)

Cu	Mn	Mg	Ti	Zr	Fe	Si	Al
5.80	0.30	0.20	0.05	0.20	0.20	0.10	Bal.

The T9I6 process for 2519A aluminum alloy in this study is depicted in Fig. 1. The T9I6 process includes solution treatment, quenching, pre-ageing, cold working, interrupted ageing, re-ageing and the T87 process is solution treatment, quenching, cold working and ageing.

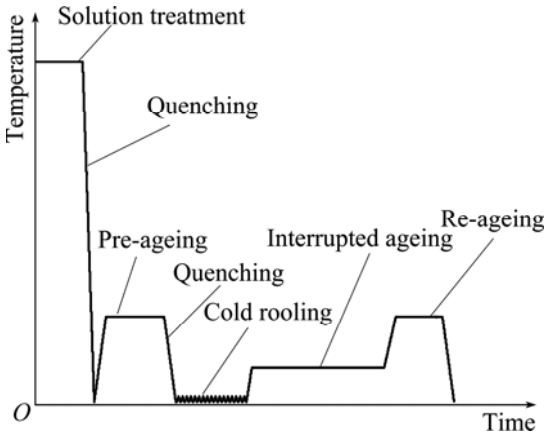

Fig. 1 Process route of T9I6 temper

The Vickers hardness was the characterization parameter. The Vickers hardness test was carried out with 3 kg loading to investigate the aging response of the alloys. Hardness reported in this study was the mean value of at least five measurements. The tensile tests were performed on MTS Landmark Servo-hydraulic Test System and conducted in air at room temperature. The stretching speed for the tensile tests was 2 mm/min. All specimens were taken in longitudinal direction from alloy plates with T87 and T9I6 tempers.

The microstructures were analyzed by optical microscopy (OM) and transmission electron microscopy (TEM, Tecnai G^2 20). The specimens for OM were etched in Keller reagent that is composed of 1.0 mL HF, 1.5 mL HCl, 2.5 mL HNO_3 and 95 mL H_2O. The samples for TEM were cut from the plate along the rolling direction. They were ground down to about 60 μm, then electro-polished in a HNO_3−CH_3OH solution (volume ratio of 3:7) at about 250 K in a twin-jet electro-poling unit.

The ballistic limit velocity is the velocity required for a particular projectile to reliably (at least 50% of the time) penetrate a particular piece of material. The ballistic limit velocity of 2519A-T9I6 alloy was tested by the ogive-shaped 7.62 mm-diameter projectile.

3 Results and discussion

3.1 Mechanical properties

The tensile properties and fracture toughness of the 2519A-T87 and 2519A-T9I6 alloys are listed in Table 1. It could be concluded that both yield strength and tensile strength of the 2519A-T9I6 alloy are enhanced compared with T87 temper. Accompanied with the increase of tensile properties, the fracture toughness of 2519A-T9I6 alloy is also higher by 4.9 $MPa·m^{1/2}$.

Table 2 Mechanical properties of 2519A-T87 and 2519A-T9I6 alloys at 298 K

Alloy	Yield strength/ MPa	Tensile strength/ MPa	Elongation/ %	Fracture toughness/ ($MPa·m^{1/2}$)
2519A-T87	431.6	470.5	9.7	27.8
2519A-T9I6	501.0	540.1	14.3	32.7

3.2 Ballistic limit velocity (v_{50}) test

The ballistic limit velocity test of the 2519A-T9I6 alloy was conducted at room temperature. The 2519A-T9I6 aluminum alloy plate (30 mm in thickness) was shot vertically at impact velocity of 818 m/s and the v_{50} was 715 m/s. Figure 2 shows the response of the plate to projectiles. Projectile embedded in the plate nearly penetrated the target (see Fig. 2(b)).

Compared with tests conducted in static or quasi-static condition, the impacted behaviors of materials are totally different. Grain morphology varies

near the sidewalls of the crater. As shown in Fig. 3(a), large grains were located around a number of small grains, which is an abnormal grain growth behavior. Abnormal grain growth happens under certain conditions, and it would lead to significant differences between the grain sizes. A few preferential growth grains annexed small grains gradually. The annexation would not stop until preferential growth grain met another abnormal growth grain. Some grains were pulled very long (see Fig. 3(b)). Adiabatic shear banding (ASB) could be found in Fig. 3(c). And micro-cracks accompanied by ASB appear in some areas. All these features mentioned above were resulted from severe deformation. The amount of dislocations multiplied rapidly due to the short deformation time in the high speed impact process. The dynamic recovery might not happen and the sub-grains might not form either. As a result, the density of the dislocation in grains was kept at a high level and the storing energy would reach the driving power of dynamic recrystallization (DRX), so all these changes in the alloy resulted in the DRX finally (Fig. 3(d)).

3.3 Microstructural evolution

It has been indicated that the precipitation reaction in Al−Cu alloys below 523 K proceeds through a well accepted sequence of transformations [15]:

$$Al_{ss}(\text{supersaturated}) \rightarrow Al_{ss}+\text{GP zones} \rightarrow Al_{ss}+\theta' \rightarrow Al_{ss}+\theta$$

where Al_{ss} represents the aluminum solid solution; the GP zones and θ' are metastable precipitate phase; θ' phase is underformable particles in 2519A aluminum morphology. A dense uniform distribution of θ' plates (Al_2Cu) with an average thickness of 3 nm is presented in aluminum matrix [16], and mechanical properties are controlled by the amount and the morphology of the θ' phase precipitated during the thermo-mechanical process. Figure 4 shows TEM images of the 2519A aluminum alloy during different treatment processes.

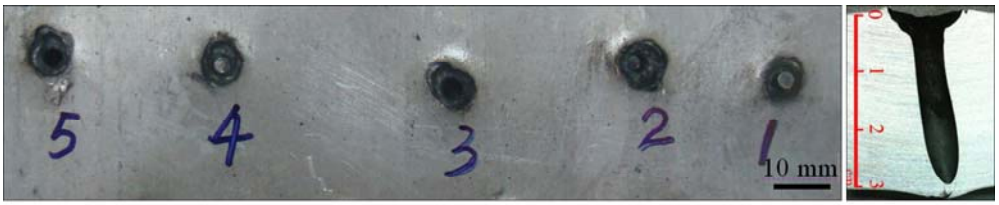

Fig. 2 Images of crater: (a) Back of plate with craters; (b) Crater profile

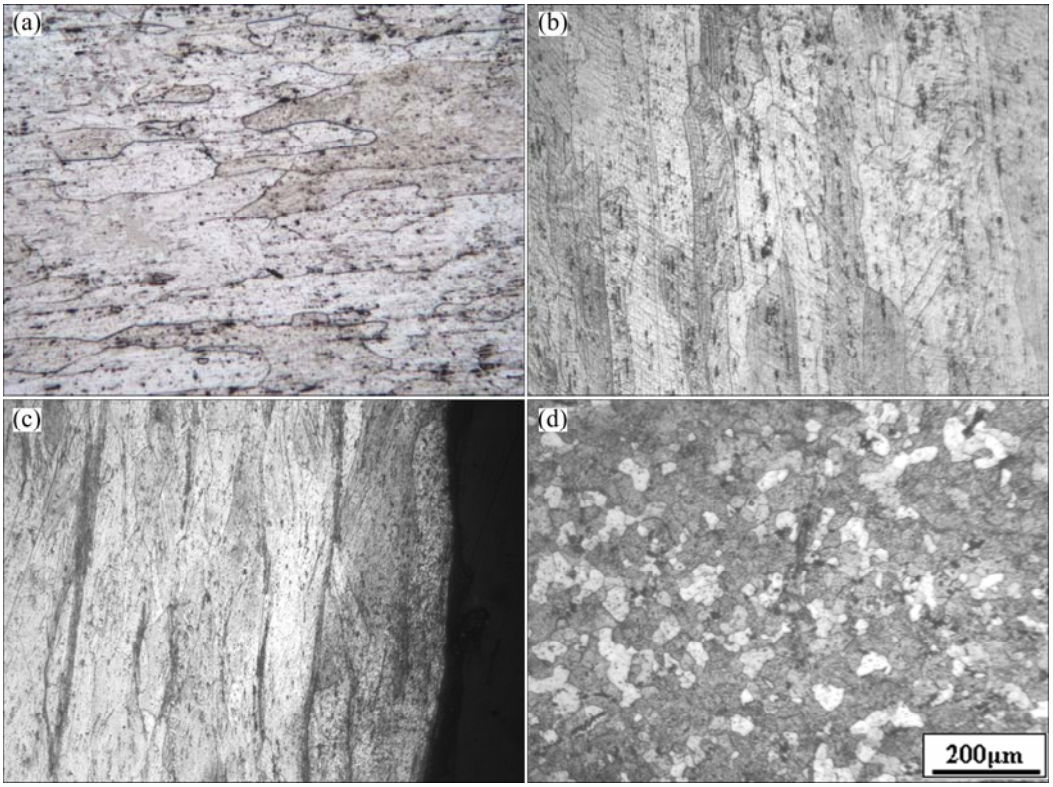

Fig. 3 Typical impacted optical microstructures: (a) Abnormal grain growth; (b) Fibrous tissue; (c) Adiabatic shear banding; (d) Dynamic recrystallization

Figures 4 (a) and (b) show that the density of the precipitate phase with T9I6 temper is higher than that with T87 temper. The SAD (selected area diffraction) patterns indicate that the precipitate phases are mainly θ' and θ phases.

Figure 4(c) shows the morphology of the precipitate phase after the interrupted period. It can only be observed under relatively high magnification. Its morphology resembles the disk shape of θ'. These tiny particles have length of 7−9 nm, and width of 0.35−0.45 nm. The particles of GP zones, according to a former study with the application of high-resolution transmission electron microscopy (HRTEM), have length about 8 nm and width about 0.4 nm [17]. Combined with the diffraction spot, these particles may be GP zones.

Aspect ratio could be used to describe the process of precipitation and transformation of the second phases in the Al−Cu alloys qualitatively. According to a former study [18], a larger aspect ratio of the precipitate phases means higher mechanical properties, such as yield strength. Area fraction and aspect ratio of precipitate phases of the studied alloy are shown in Fig. 5. The area fraction of 2519A-T9I6 alloy, which is 30.24%, is 1.5 times that of the 2519A-T87 alloy. The colored areas illustrate the different aspect ratios in these precipitate phases. Among these, aspect ratios ranging in 0−10 as well as those ranging in 10−20 gain the dominant position in 2519A-T87 alloy. In the result of T9I6 process, the aspect ratio is mainly in the range of 10−20. Besides, aspect ratio over 30 could also be found. That is to say, more strengthening phase can be found in 2519A-T9I6.

Under T9I6 processing condition, pre-ageing works the same way with the T6 ageing. The following cold rolling introduces work hardening, lending a higher starting point for the following ageing strengthening; on the other hand, it increases dislocation density of the matrix, decreases the lattice distortion energy, thus providing conditions for the θ' phase nucleation on half coherent Al matrix.

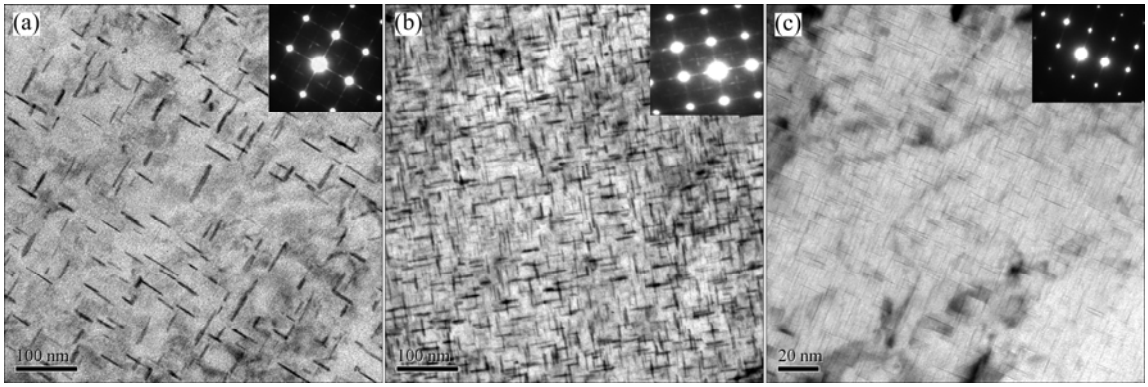

Fig. 4 TEM images and corresponding SAD patterns of 2519A aluminum alloy during different treatment processes: (a) Peak ageing at T87 temper, (b) Peak ageing at T9I6 temper; (c) After interrupted ageing period

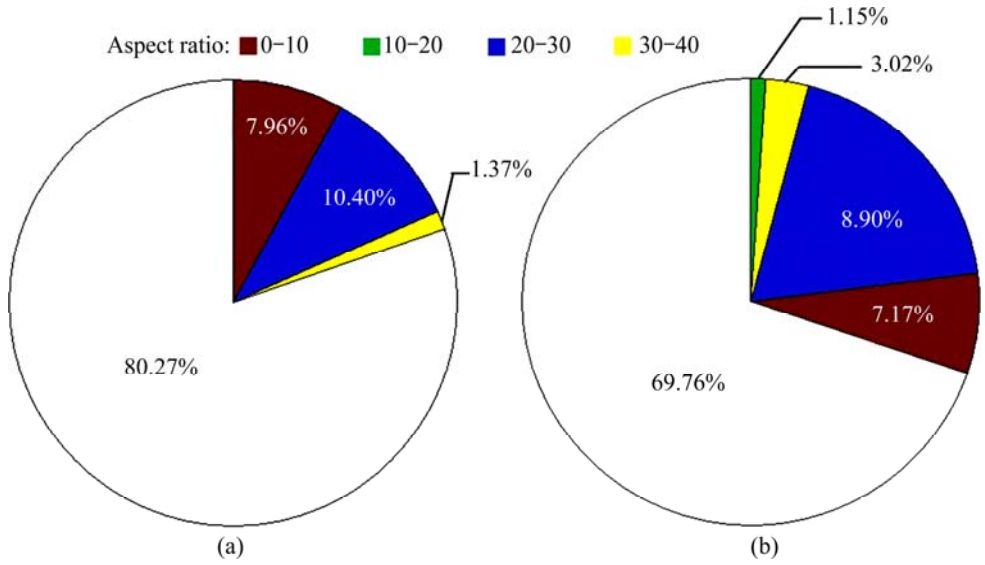

Fig. 5 Area fraction of precipitate phase of 2519A aluminum alloy treated with T87 (a) and T9I6 (b) temper

In the procedure of low temperature insulation, the super saturation of the matrix increases, and the free energy of phase changing of GP zones increases. Meanwhile, the diffusion rate of the solvent atoms under relatively low temperature is low, thus obtaining uniformity of nucleation in GP zone. After reaching certain size, these GP zones become the crystal core of the following ageing precipitate phase [9].

What's more, during the interrupted period, Cu atoms segregated to a large amount of Cu-rich GP zones, while their migration speed reduced due to low temperature. As a result, only minor amount of Cu atoms diffuse to grain boundaries and subboundaries. Thus, the amount of precipitation at the grain boundaries is relatively small, alloys are then less easily to produce micro-fissure while deforming. Because of this, compared with the alloys at T87 temper, they have improvements in plasticity and toughness under the temper of T9I6. This is parallel to the former results.

3.4 Orowan strengthening in 2519A-T9I6 alloy

Dislocations would bypass or cut the particles of the second phase according to the size of particles. These two ways of dislocation motion were summarized as two different mechanisms. The critical shear stress of these mechanisms was affected by the volume fraction and size of the second phase particles. The relationship between the radius of the second phase and strengthening effect of these two mechanisms is shown in Fig. 6. The Orowan mechanism indicated that critical shear stress for dislocations to bypass the particles is [19]

$$\Delta\tau_{\text{bypass}} \propto \frac{Gbf^{1/2}}{r}\ln\left(\frac{2r}{r_0}\right) \approx \alpha f^{1/2} r^{-1} \tag{1}$$

and that for dislocations to cut the particles is

$$\Delta\tau_{\text{Cut}} \propto f^{1/2\sim5/6} r^{1/2} \approx \beta f^{n} r^{1/2} \tag{2}$$

where f is the fraction of the second phase, and r is the radius of it. The effect of strengthening would be the most remarkable at point of intersection of the lines shown in Fig. 5, and the best radius of the particles is r_c. It could be estimated that the r_c of 2519A aluminum alloy is 3−10 nm. It could be known from Fig. 4 that the radius of θ' phase in 2519A is much smaller than the calculated value and the Orowan mechanism worked mainly during T87 and T9I6 processes. Orowan strengthening, caused by the resistance of closely spaced hard particles to the passing of dislocations, is important in aluminum alloys. A larger fraction of the second phase (f) and a smaller size(r) of particles would contribute to the strengthening of alloys. T9I6 temper, together with a larger θ' phase fraction and thinner particles compared with T87 temper, has an obvious strengthening effect.

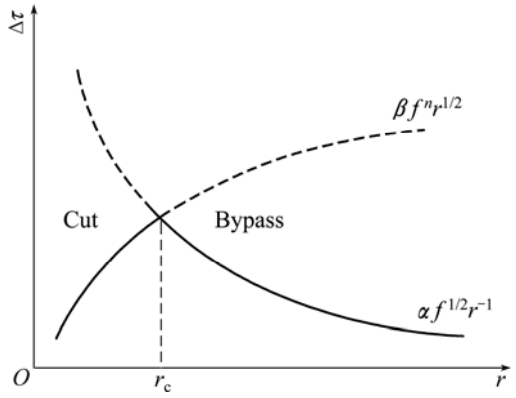

Fig. 6 Relationship between radius of the second phase and strengthening effect

4 Conclusions

1) After the T9I6 thermo-mechanical process, the yield strength, tensile strength, elongation of 2519A-T9I6 aluminum alloy reach 501 MPa, 540 MPa and 14%, respectively. All these mechanical properties increase sharply compared with 2519A-T87.

2) The ballistic limit velocity of the 2519A-T9I6 alloy (30 mm in thickness) is 715 m/s. And typical impacted optical microstructures could be found in the alloy.

3) Interrupted period is the key to the enhancement. The θ' phase is denser and finer during the interrupted ageing period and contributes to better properties of the 2519A-T9I6 alloy.

References

[1] ZHANG Xin-ming, JIA Yu-zhen, LIU Ling, YE Ling-ying, CHEN Ming-an, GAO Zhi-guo, WANG Wen-tao, KUANG Xiao-yue. Effects of cold-pre-rolling reduction on precipitation of 2519A aluminum alloy plate [J]. Journal of Central South University: Science and Technology, 2011, 42(1): 46−49. (in Chinese)

[2] ZHANG Xin-ming, LI Hui-jie, LI Hui-zhong, GAO Hui, GAO Zhi-guo, LIU Ying, LIU Bo. Dynamic property evaluation of aluminum alloy 2519A by split Hopkinson pressure bar [J]. Transactions of Nonferrous Metals Society of China, 2008, 18(1): 1−5.

[3] ZHANG Xin-ming, LIU Ling, JIA Yu-zhen. Effects of stretching and rolling pre-deformation on microstructures and mechanical properties of 2519A aluminum alloy [J]. The Chinese Journal of Nonferrous Metals, 2010, 20(6): 1088−1094. (in Chinese)

[4] LI Hui-zhong, LIANG Xiao-peng, CHEN Ming-an, ZHANG Xin-ming. Effect of cold rolling reduction on microstructure and mechanical property of 2519 aluminum alloy [J]. Transactions of Material and Heat Treatment, 2010, 20(6): 1088−1094.

[5] LI Hui-zhong, LIANG Xiao-peng, LI Fang-fang, GUO Fei-fei, LI Zhou, ZHANG Xin-ming. Effect of Y content on microstructure and mechanical properties of 2519 aluminum alloy [J]. Transactions of Nonferrous Metals Society of China, 2007, 17(6): 1194−1198.

[6] WANG Wen-tao, ZHANG Xin-ming, GAO Zhi-guo, JIA Yu-zhen, YE Ling-ying, ZHENG Da-wei, LIU Ling. Influences of Ce addition

on the microstructures and mechanical properties of 2519A aluminum alloy plate [J]. Journal of Alloys and Compounds, 2010, 419(1−2): 366−371.

[7] ZHANG Xin-ming, WANG Wen-tao, CHEN ming-an, GAO Zhi-guo, JIA Yu-zhen, YE Ling-ying, ZHENG Da-wei, LIU Ling, KUANG Xiao-yue. Effects of Yb addition on microstructures and mechanical properties of 2519A aluminum alloy plate [J]. Transactions of Nonferrous Metals Society of China, 2010, 20(5): 727−731.

[8] LOEFFLER H, KOVACS I, LENDVAI J. Decomposition processes in Al−Zn−Mg alloys [J]. Journal of Materials Science, 1983, 18(8): 2215−2240.

[9] LUMLEY R N, POLMEAR I J, MPRTON A J. Temper developments using secondary ageing [C]//NIE J F, MORTON A J, MUDDLE B C. Proceedings of the 9th International Conference on Aluminum Alloys. Brisbane, Australia: Institute of Materials Engineering Australasia Ltd, 2004: 85−95.

[10] LUMLEY R N, POLMEAR I J, MPRTON A J. Interrupted aging and secondary precipitation in aluminum alloys [J]. Materials Science and Technology, 2003, 19(11): 1483−1490.

[11] LUMLEY R N, POLMEAR I J, MPRTON A J. Development of mechanical properties during secondary aging in aluminum alloys [J]. Materials Science and Technology, 2005, 21(9): 1025−1032.

[12] HAN Nian-mei, ZHANG Xin-ming, LIU Sheng-dan, SONG Feng-xuan, XIN Xing. Influence of two-step aging on fracture toughness of 7050 aluminum alloy plate [J]. Journal of Central South University: Science and Technology, 2011, 42(3): 623−628. (in Chinese)

[13] ZHANG Xin-ming, SONG Feng-xuan, LIU Sheng-dan, HAN Nian-mei. Influence of two-step aging on exfoliation corrosion properties of 7050 aluminum alloy plate [J]. Journal of Central South University: Science and Technology, 2011, 42(8): 2252−2258. (in Chinese)

[14] YU Li-jun, ZHENG Zi-qiao, LI Shi-chen, LIU Gang, WEI Xiu-yu. Effects of heat treatment T6I6 on microstructures and properties of 2195 alloy [J]. Transactions of Materials and Heat Treatment, 2006, 27(5): 79−83. (in Chinese)

[15] VAITHYANATHAN V, WOLVERTON C, CHEN L Q. Multiscale modeling of θ' precipitation in Al−Cu binary alloys [J]. Acta Materialia, 2004, 52(10): 2973−2987.

[16] LI Song-rui, ZHOU Shan-chu. Heat treatment of metals [M]. Changsha: Central South University Press, 2005: 198−202. (in Chinese)

[17] TAKEDA M, MAEDA Y, YOSHIDA A, YABUTA K, KONUMA S, ENOO T. Discontinuity of GP (I) zone and θ'-phase in an Al−Cu alloy [J]. Scripta Materialia, 1999, 41(6): 643−649.

[18] GAO Zhi-guo, ZHANG Xin-ming, CHEN Min-an. Influence of strain rate on the precipitate microstructure in impacted aluminum alloy [J]. Scripta Materialia, 2008, 9(59): 983−986.

[19] ZHENG Zi-qiao. Material science and engineering [M]. Changsha: Central South University Press, 2005: 478−481. (in Chinese)

T9I6 形变热处理工艺对 2519A 铝合金组织、力学性能及抗弹性能的影响

顾 刚[1,2]，叶凌英[1,2]，蒋海春[1,2]，孙大翔[1,2]，张 盼[1,2]，张新明[1,2]

1. 中南大学 材料科学与工程学院，长沙 410083；
2. 中南大学 有色金属材料科学与工程教育部重点实验室，长沙 410083

摘 要：借助金相显微镜、透射电镜、拉伸测试、抗弹性能测试等手段研究 T9I6 新型形变热处理对 2519A 铝合金组织、力学性能和抗弹性能的影响。经 T9I6 工艺处理的 2519A 铝合金，其屈服强度、抗拉强度、伸长率分别达到 501 MPa、540 MPa、14%。30 mm 厚的 2519A-T9I6 铝合金板材的极限穿透速度达 715 m/s。弹坑侧壁组织随着弹孔深度的变化而变化。T9I6 热处理工艺中的断续时效阶段是 2519A 铝合金性能提升的关键。低温下的时效使得 GP 区变得密集，从而使得后续相的析出也变得更为密集、细小。

关键词：2519A 铝合金；T9I6 形变热处理工艺；力学性能；微观组织；抗弹性能

(Edited by Xiang-qun LI)